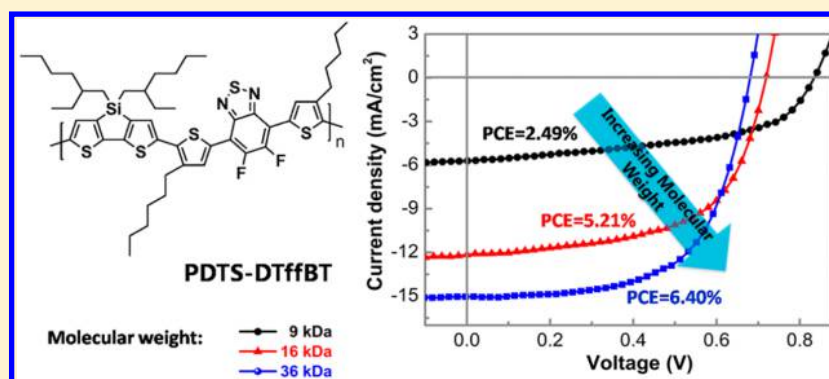


Optimization of PDTS-DTffBT-Based Solar Cell Performance through Control of Polymer Molecular Weight

Pengfei Ma,[†] Shanpeng Wen,^{*,†,‡} Chen Wang,[†] Wenbin Guo,[†] Liang Shen,[†] Wei Dong,[†] Jingbin Lu,[†] and Shengping Ruan^{*,‡}

[†]State Key Laboratory on Integrated Optoelectronics and College of Electronic Science & Engineering, Jilin University, Changchun 130012, P. R. China

[‡]State Key Laboratory on Applied Optics, Changchun 130012, P. R. China



ABSTRACT: Herein, we investigated the effect of molecular weight (MW) on the efficiency of PDTS-DTffBT based polymer solar cells (PSCs). PDTS-DTffBTs with three different MWs were synthesized by controlling the polymerization conditions. The performance of PSCs improved significantly as the number-average molecular weight (M_n) increased from 9 to 36 kDa. Combined with UV-vis absorption and electrochemical cyclic voltammetry measurements, the absorption properties and frontier orbital energy levels of the polymers were estimated, indicating the red-shifted light absorption and up-shifted highest occupied molecular orbital (HOMO) energy level when MW increased. PDTS-DTffBT with high MW also provided increased charge mobility, smoother film surface, and reduced domain size in morphology of the PDTS-DTffBT:PC₇₁BM active layer. The performance of PDTS-DTffBT based PSCs was improved owing to these MW related properties, and both short circuit current density (J_{SC}) and power conversion efficiency (PCE) went up significantly with increasing MW. The best PCE of 6.40% was achieved by the devices based on the PDTS-DTffBT with a M_n value of 36 kDa.

1. INTRODUCTION

Polymer solar cells (PSCs) have attracted much attention because of their potentials for low cost, easy processing, light weight, flexibility, and large-area fabrication.^{1–4} Bulk heterojunction (BHJ) PSCs based on polymer:PCBM blends have improved significantly in terms of power conversion efficiency (PCE) over the past decades.^{5–8} Among polymer:PCBM blend films, the polymer materials are of vital importance because they determine not only the maximum attainable short-circuit current density (J_{SC}) but also the largest open-circuit voltage (V_{OC}).^{9–11} Therefore, the development of low bandgap polymers with deep highest occupied molecular orbital (HOMO) energy level has been one of the crucial factors for the improvement of PCE in PSCs.

Donor-acceptor (D-A) copolymer has been proven to be an efficient strategy to synthesize low bandgap polymers for photovoltaic applications.^{12–14} For D-A copolymer, donor and acceptor units are alternatively copolymerized with each other, forming an intramolecular charge transfer (ICT) state, and the structure of energy levels as well as the optical bandgap can be

tuned and optimized so as to match well with both the energy levels of PCBM in the BHJ blend and the solar spectrum.^{15,16} It is known from the fundamentals of physical chemistry that the strength of ICT states varies between different donor and acceptor units, and it is also demonstrated that the practical performance changes a lot when we change the donor and acceptor units.^{17–19} All of these illustrate that the choice of appropriate donor and acceptor units plays a critical role. By using this way, many novel D-A type conjugated copolymers, containing a large conjugated donor unit and a strong electron acceptor unit, have been successfully developed and used in PSCs with PCE over 10%.^{20–22}

It is a notable fact that polymer-based solar cells still show different performance, although they have the same donor and acceptor units as well as molecular backbone.^{23–25} It is known that polymers normally have varying molecular weight (MW)

Received: May 24, 2016

Revised: August 16, 2016

Published: August 23, 2016

and polydispersity index (PDI) from batch to batch, and this low reproducibility is caused by the complicated synthesis itself.²⁶ The MW can influence physical properties of polymers, for instance, HOMO/LUMO energy levels, optical bandgap, the conjugation length, and charge transport mobility.^{27–29} As all of these factors determine the photovoltaic performance of the solar cells, PSCs usually demonstrate considerably different behaviors in terms of J_{SC} , V_{OC} , and fill factor (FF), which have been observed and reported by different research groups.^{30–34} For instance, Schilinsky et al. observed that the efficiency increases about 10–20-fold and short circuit current goes up 5–10-fold for the P3HT:PCBM based solar cells when P3HT is made of higher MW fractions (13.8–19 kDa) compared with lower MW fractions (2.2–5.6 kDa), which is caused by the reduced hole mobility of lower MW samples.³⁵ Chu et al. reported that the efficiency goes up to 7.7% for PDTSTPD based solar cells when the number-average molecular weight (M_n) is as high as 31 kDa. It was explained that higher MW leads to higher hole mobility, strong light absorption intensity, and lower device series resistance.³⁶ In addition, MW also influences the micromorphology of the active layer.^{37–39} Bertel et al. have observed that, as the MW increased, the size of the PC₇₀BM-rich domain was decreased following the formation of a fibrillar network during spin-coating, and the device performance was increased accordingly.⁴⁰ The above advantages of high MW polymers highlight the significance of achieving high MW polymers for improving device performance.

Recently, we reported a new D–A copolymer of poly{4,4'-bis(2-ethylhexyl)dithieno[3,2-*b*:2',3'-*d*]silole-*alt*-5,6-difluoro-4,7-bis(4-hexylthiophen-2-yl)-2,1,3-benzothiadiazole} (PDTSDTffBT) containing dithieno[3,2-*b*:2',3'-*d*]silole (DTS) and fluorinated benzothiadiazole (DTffBT) units.^{41,42} PDTSDTffBT showed a broad absorption spectrum from 300 to 800 nm and a relatively low-lying HOMO energy level of –5.28 eV. Preliminary devices based on the blend of PDTSDTffBT with PC₇₁BM provided a promising initial PCE of 5.26%. Herein, we investigated the influence of MW on the performance of PDTSDTffBT based PSCs. PDTSDTffBT with three different MWs (M_n = 9, 16, 36 kDa) were synthesized. It was found that, with the increasing MW, the HOMO energy level of PDTSDTffBT goes up, causing the decrease in bandgap. Meanwhile, both the hole mobility and morphology were improved for the PDTSDTffBT:PC₇₁BM active layer where the MW of PDTSDTffBT is higher. All of these factors contribute together to a higher PCE of 6.40% and enhanced J_{SC} for the solar cells based on PDTSDTffBT with high MW.

2. EXPERIMENTAL SECTION

2.1. Measurements and Characterization. The MWs were determined by gel permeation chromatographic (GPC) analysis referenced to polystyrene using a Waters 410 instrument with tetrahydrofuran (THF) as the eluent (flow rate: 1 mL min^{–1}, 35 °C). ¹H NMR spectra were collected on a Bruker AVANCE 600 MHz spectrometer or Bruker 400 MHz DRX spectrometer in chloroform-*d* solvent referenced to tetramethylsilane (TMS). Elemental analysis was performed with an Elementar vario EL cube elemental analyzer. The UV–vis absorption spectra were acquired on a Shimadzu UV-3600 spectrophotometer. The thin films were fabricated by spin-coating the polymers onto quartz substrates from 10 mg/mL polymer solutions in 1,2-dichlorobenzene (DCB), and a Veeco

DEKTAK 150 surface profilometer was employed to measure the film thickness. Cyclic voltammetry measurement was carried out on a Bioanalytical Systems BAS 10 B/W electrochemical workstation.

2.2. Materials. Unless otherwise stated, all materials were purchased from Aldrich and used without further purification. Prior to synthesis, toluene was purified by distillation from sodium/benzophenone and *N,N*-dimethylformamide (DMF) was distilled from CaH₂ under nitrogen. The monomers, 4,4'-bis(2-ethylhexyl)-5,5'-bis(trimethyltin)-dithieno[3,2-*b*:2',3'-*d*]silole (monomer 1) and 5,6-difluoro-4,7-bis(5-bromo-4-hexylthiophen-2-yl)-2,1,3-benzothiadiazole (monomer 2), were synthesized according to literature procedures.⁴¹

Synthesis of PDTSDTffBT. 4,4'-Bis(2-ethylhexyl)-5,5'-bis(trimethyltin)-dithieno[3,2-*b*:2',3'-*d*]silole (monomer 1, 193 mg, 0.259 mmol), 5,6-difluoro-4,7-bis(5-bromo-4-hexylthiophen-2-yl)-2,1,3-benzothiadiazole (monomer 2, 172 mg, 0.259 mmol), anhydrous toluene (6 mL), and DMF (1 mL) were mixed and purged with nitrogen for 30 min in a two-neck round-bottom flask (25 mL). After adding Pd(PPh₃)₄ (15 mg), the mixture was stirred under nitrogen at 110 °C for 32 h. The mixture was cooled to room temperature followed by precipitated in methanol. The precipitated solid was filtered through a Soxhlet thimble and washed sequentially with methanol, hexane, and chloroform in a Soxhlet extractor. Finally, the fraction from chloroform was concentrated under reduced pressure, precipitated into methanol, and collected by filtration to yield the final polymer with 36 kDa as a black solid (195 mg, 82% yield). A similar synthetic procedure was followed for the preparation of 16 and 9 kDa fractions with slight modifications: the 16 kDa fraction was stirred at 110 °C for 28 h (78% yield), while the 9 kDa fraction was stirred at 95 °C for 24 h (64% yield).

PDTSDTffBT (9 kDa). GPC: M_n = 9000 g/mol, M_w = 12 150 g/mol, PDI = 1.35; ¹H NMR (400 MHz, CDCl₃, TMS): δ (ppm) 8.14 (br, 2H), 7.08 (br, 2H), 2.90 (br, 4H), 1.76 (br, 4H), 1.64–1.16 (m, 30H), 1.05 (br, 4H), 1.01–0.73 (m, 18H). Anal. Calcd for C₅₀H₆₄F₂N₂S₅Si: C, 65.31; H, 7.02; F, 4.13; N, 3.05; S, 17.44; Si, 3.05. Found: C, 64.53; H, 7.08; N, 2.85; S, 16.93.

PDTSDTffBT (16 kDa). GPC: M_n = 16 000 g/mol, M_w = 24 320 g/mol, PDI = 1.52; ¹H NMR (600 MHz, CDCl₃, TMS): δ (ppm) 8.10 (br, 2H), 7.10 (br, 2H), 2.88 (br, 4H), 1.77 (br, 4H), 1.64–1.18 (m, 30H), 1.07 (br, 4H), 1.02–0.75 (m, 18H). Anal. Calcd for C₅₀H₆₄F₂N₂S₅Si: C, 65.31; H, 7.02; F, 4.13; N, 3.05; S, 17.44; Si, 3.05. Found: C, 64.68; H, 7.04; N, 2.87; S, 17.06.

PDTSDTffBT (36 kDa). GPC: M_n = 36 000 g/mol, M_w = 101 880 g/mol, PDI = 2.83; ¹H NMR (400 MHz, CDCl₃, TMS): δ (ppm) 8.13 (br, 2H), 7.12 (br, 2H), 2.89 (br, 4H), 1.76 (br, 4H), 1.64–1.16 (m, 30H), 1.04 (br, 4H), 1.01–0.73 (m, 18H). Anal. Calcd for C₅₀H₆₄F₂N₂S₅Si: C, 65.31; H, 7.02; F, 4.13; N, 3.05; S, 17.44; Si, 3.05. Found: C, 65.16; H, 7.10; N, 2.83; S, 17.14.

2.3. Polymer Solar Cell Fabrication and Characterization. PSCs were prepared by employing a conventional device configuration with ITO/PEDOT:PSS as the anode, PDTSDTffBT:PC₇₁BM as the active layer, and LiF/Al as the cathode. First, we conducted ultrasonic cleaning for the patterned ITO substrates (15 Ω /square) using detergent, deionized water, acetone, and isopropyl alcohol sequentially. Then, these ITO glasses were treated by UV-ozone for 10 min. After that, a PEDOT:PSS (Clevious P VP AI 4083) water

dispersion was dropped onto the ITO surface (passed through a 0.22 μm filter) and spin-coated at 5000 rpm for 50 s. The PEDOT:PSS films were heated on a hot plate (140 $^{\circ}\text{C}$) in the atmosphere for 30 min to give a thin film with a thickness of ~ 40 nm. We dissolved 10 mg of polymers (with different MWs) and 20 mg of PC₇₁BM in a mixed solvent containing 970 μL of DCB and 30 μL of 1,8-diiodooctane (DIO) and stirred the blend solution for 24 h before using. The aforementioned solutions were filtered and then spin-coated above the PEDOT:PSS film in an argon-filled glovebox using 700–1200 rpm for 50 s to obtain a similar film thickness of ~ 95 nm for the three different MW fractions. Then, the devices were heated at 120 $^{\circ}\text{C}$ for 5 min in a glovebox. Finally, the 0.6 nm LiF and 100 nm aluminum cathode was formed by the thermal evaporation method. A shadow mask was used to obtain an about 6.4 mm² effective area.

A Keithley 2400 Source Meter was used to measure the J - V curves of the final devices working under dark and AM 1.5 G solar irradiation (the light intensity of the Oriel 300 W solar simulator is 100 mW/cm², and this was tested by an IL1400 photometer and calibrated by a standard silicon solar cell). The external quantum efficiency (EQE) curves were measured utilizing a Crowntech QTest Station 1000 AD. Mobility measurements were performed by the space-charge limited current (SCLC) method. The devices were prepared in the hole-only configuration with ITO/PEDOT:PSS and Au as electrodes on both sides. The hole mobility can be calculated by fitting the resulting curves to a space-charge-limited form. Atomic force microscopy (AFM) images were obtained with a Veeco Dimension 3100 instrument working at tapping mode. Unless otherwise specified, it is in air and at room temperature that these tests were performed.

3. RESULTS AND DISCUSSION

The PDTS-DTffBTs with different MWs were obtained by varying the reaction conditions (see the [Experimental Section](#)), and the chemical structure as well as the polymerization of PDTS-DTffBT are shown in [Figure 1](#). The M_n 's of the resulting polymers were measured to be 9, 16, and 36 kg/mol with a PDI of 1.35, 1.52, and 2.83, respectively.

3.1. Photophysical Properties. The UV-vis absorption spectra of these different MW PDTS-DTffBTs in chloroform solutions and in films are shown in [Figure 2](#), and the main parameters are listed in [Table 1](#). In dilute solution, all of the polymers exhibited spectral tails extending to 700 nm. As the

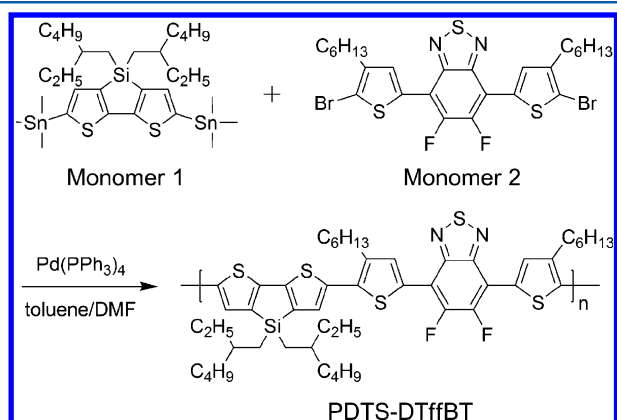


Figure 1. Chemical structure and synthesis of PDTS-DTffBT.

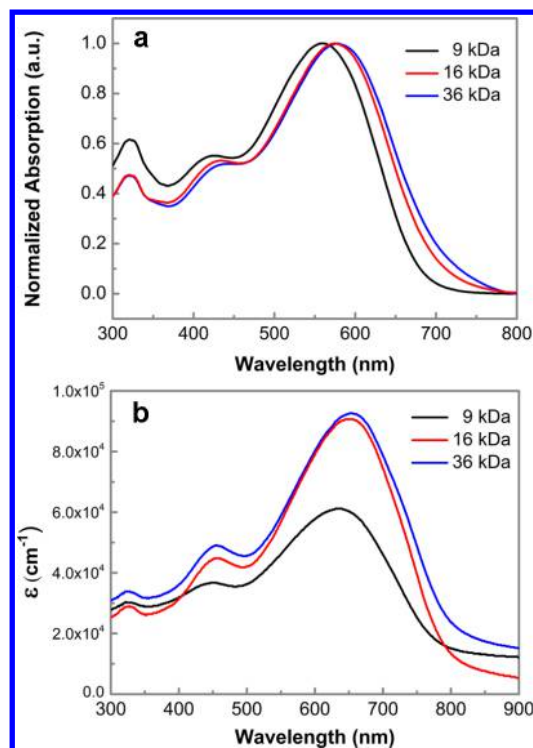


Figure 2. UV-vis absorption spectra of PDTS-DTffBTs in (a) chloroform and (b) solid film with different molecular weights.

MW increased from 9 to 36 kDa, the maximum absorption peak red-shifted from 560 to 579 nm and the absorption edge red-shifted from 679 to 709 nm because of the increased conjugation length.⁴³ However, the maximum absorption peaks and absorption edges of PDTS-DTffBTs with M_n 's of 16 and 36 kDa were almost similar, indicating that the effective conjugation length of the polymer main chain was nearly saturated.⁴⁴ The thin film absorption of different MW PDTS-DTffBTs exhibited a similar trend to that in solution. The maximum peaks and absorption edges red-shifted as the MW increased. The optical bandgaps of polymers were 1.61, 1.58, and 1.57 eV for a M_n of 9, 16, and 36 kDa, respectively, calculated from the absorption edges of the thin solid film. The absorption coefficients were also increased along with the MW increasing, which was likely a result of more ordered stacking and denser film for high MW PDTS-DTffBTs.⁴⁵

3.2. Electrochemical Properties. We used electrochemical cyclic voltammetry to characterize the HOMO and LUMO energy levels of the polymers. The measurements were performed under a N₂ atmosphere, in acetonitrile containing 0.1 M tetrabutylammonium hexafluorophosphate as the supporting electrolyte, with a platinum button coated with polymer film as the working electrode, platinum wire as the counter electrode, Ag/AgNO₃ as the reference electrode, and ferrocene/ferrocenium (Fc/Fc⁺) as the internal standard.

[Figure 3](#) presents the measured redox curves of ferrocene and the PDTS-DTffBTs. Taking Ag/AgNO₃ as a reference, the formal potential was determined to be 0.09 V for Fc/Fc⁺. Assuming that the energy level of Fc/Fc⁺ is located at 4.8 eV below the vacuum level, we evaluate the HOMO and LUMO energy levels of PDTS-DTffBTs according to the following equations^{46,47}

$$\text{HOMO (eV)} = -e(E_{\text{ox}}^{\text{onset}} + 4.71)$$

Table 1. Photophysical and Electrochemical Properties of PDTS-DTffBTs

M_n (kDa)	$\lambda_{\text{max}}^{\text{sol}}$ (nm)	$\lambda_{\text{max}}^{\text{film}}$ (nm)	ϵ^{film} (cm^{-1})	E_g^{opt} (eV)	$E_{\text{ox}}^{\text{onset}}$ (V)	HOMO (eV)	$E_{\text{reg}}^{\text{onset}}$ (V)	LUMO (eV)	E_g^{ec} (eV)
9	560	633	6.12×10^4	1.61	0.66	-5.37	-1.01	-3.70	1.67
16	575	646	9.06×10^4	1.58	0.57	-5.28	-1.05	-3.66	1.62
36	579	651	9.26×10^4	1.57	0.54	-5.25	-1.06	-3.65	1.60

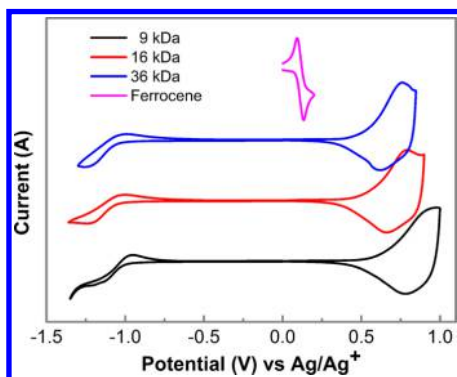


Figure 3. Cyclic voltammograms of PDTS-DTffBTs with different molecular weights.

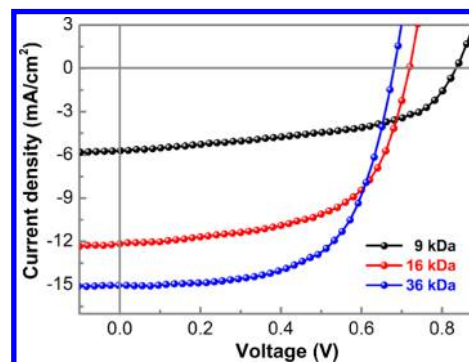
$$\text{LUMO (eV)} = -e(E_{\text{red}}^{\text{onset}} + 4.71)$$

$$E_g^{\text{ec}} \text{ (eV)} = e(E_{\text{ox}}^{\text{onset}} - E_{\text{red}}^{\text{onset}})$$

where $E_{\text{ox}}^{\text{onset}}$ and $E_{\text{red}}^{\text{onset}}$ are the measured onset potentials relative to Ag/Ag^+ .

Table 1 shows the measurement results of the HOMO and LUMO energy levels of the polymers. We find that the HOMO energy level exhibits a positive dependence on molecular weight, rising from -5.37 to -5.25 eV as M_n increased from 9 to 36 kDa. The different HOMO energy levels may result in different V_{OC} 's for PSCs based on these fractions, since the V_{OC} is determined by the energy gap between the HOMO of the polymer donor and the LUMO of the PCBM acceptor.^{48,49} As for the LUMO energy levels, the variation amplitude was relatively smaller, which indicates that the decrease of the bandgap as the MW increased was mainly caused by the increased HOMO energy level. The lowest bandgap was evaluated to be 1.60 eV in the case of 36 kDa PDTS-DTffBT, and the bandgap results determined here were slightly larger than those optical bandgap results.

3.3. Photovoltaic Properties. In order to reveal the effects of MW on the photovoltaic properties of PDTS-DTffBT, BHJ PSCs employing an ITO/PEDOT:PSS/PDTS-DTffBT:PC₇₁BM/LiF/Al device configuration were prepared and examined under simulated 100 mW cm^{-2} AM 1.5G illumination. For fair comparison, three types of devices adopted uniform concentration, polymer:fullerene weight ratio, processing solvent, solvent additive, etc., as we reported previously.⁴¹ The detailed process for device fabrication was described in the Experimental Section. Figure 4 shows the J - V curves of BHJ PSCs fabricated from polymers with different MWs, and Figure 5 shows the error bars of photovoltaic parameters of the PSCs. The corresponding parameters are summarized in Table 2. It can be seen that the MW of polymers showed a clear impact on the photovoltaic performance including V_{OC} , J_{SC} , FF, and thus PCE. The V_{OC} suffered an apparent decline as the MW increased from 9 to 16 kDa, which corresponds with the up-shifted HOMO energy levels as estimated by cyclic voltammetry measurement and it can be

Figure 4. J - V curves of the polymer solar cells based on different molecular weight PDTS-DTffBT:P₇₁CBM under AM 1.5G irradiation (100 mW cm^{-2}).

explained by the increased conjugation length.⁴⁴ Further increase of the MW to 36 kDa only led to a 40 mV decrease in V_{OC} , indicating a saturated conjugation length. As a result, the 9 kDa PDTS-DTffBT based device exhibited the highest V_{OC} of 0.83 V among this series. However, the final PCE of PSCs based on 9 kDa PDTS-DTffBT was much lower than that of the other two high MW fractions. Remarkably increased PCEs of 5.21 and 6.40% were obtained from devices based on high MW PDTS-DTffBTs (16 and 36 kDa, respectively), benefiting from the enhanced FFs and more than 2-fold J_{SC} 's. This can be attributed to the substantially enhanced absorption coefficient, more favorable nanoscale morphology, and concomitant increase in charge carrier mobility (see below). By contrast, the efficiency difference between the 16 and 36 kDa PDTS-DTffBT based devices was relatively small and primarily influenced by the J_{SC} which increased from 12.16 to 15.04 mA/cm^2 . Figure 6 presents EQE curves of the PSCs in which the spectral dependence of photocurrent can be examined. The broad EQE response range of 300–800 nm agreed well with absorption spectra of PDTS-DTffBTs with different MWs. Clearly, the low MW polymer based device offered the lowest EQE value (less than 30%) due to its poor light harvesting. As the MW increased, the EQE curves were significantly improved with the peak EQE value up to 54.3 and 63.6% for 16 and 36 kDa, respectively. The EQE gain can only be partly ascribed to the preferable optical absorbance of polymers because of the similar optical absorbance between 16 and 36 kDa PDTS-DTffBT. The EQE curve of the device made from the 36 kDa fraction showed an apparent improvement covering the whole response region over that of the 16 kDa fraction based device, meaning that more efficient exciton dissociation and/or charge collection took place. This promoted us to find out further supportive evidence by investigating the film morphology and carrier mobility of devices.

3.4. Charge Mobility. To further understand the reasons behind the promoted device performance as the MW increased, the hole mobilities of three MW fractions were measured by using the SCLC method.⁵⁰ The devices were prepared in the hole-only configuration with ITO/PEDOT:PSS and Au as

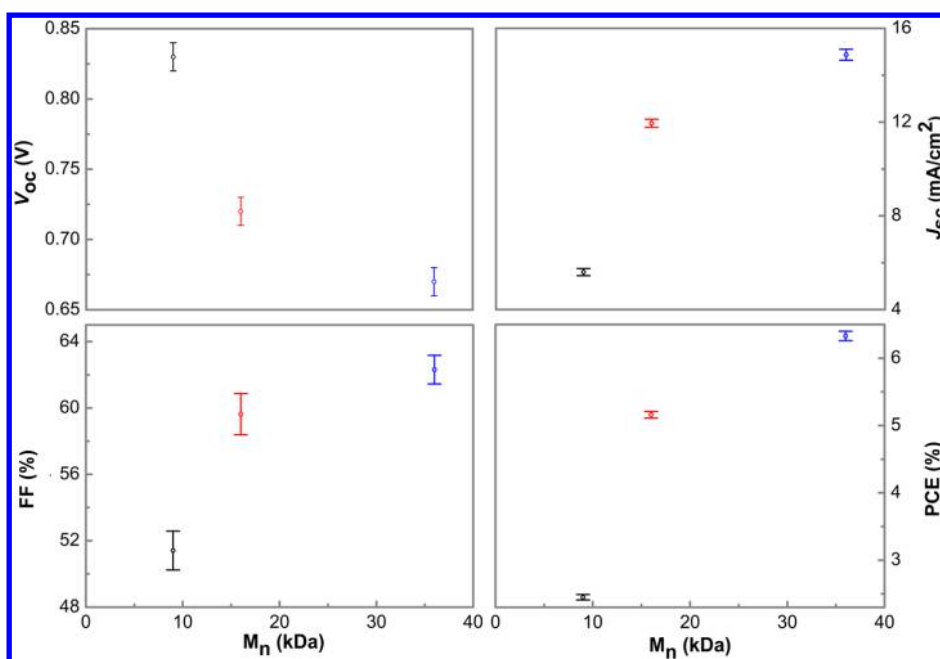


Figure 5. Error bars of photovoltaic parameters of PSCs based on PDTs-DTffBT with different molecular weights.

Table 2. Photovoltaic Parameters of the BHJ Solar Cells Based on PDTs-DTffBT with Different Molecular Weights and the Hole Mobility of the Blend Films

M_n (kDa)	V_{OC} (V)	J_{SC} (mA cm ⁻²)	FF (%)	PCE (%)	μ_h (cm ² V ⁻¹ s ⁻¹)
9	0.83 ± 0.01	5.75 ± 0.15	51.41 ± 1.17	2.49 (2.45)	4.76 × 10 ⁻⁵
16	0.72 ± 0.01	12.01 ± 0.17	59.63 ± 1.24	5.21 (5.16)	1.47 × 10 ⁻⁴
36	0.67 ± 0.01	14.89 ± 0.23	62.31 ± 0.86	6.40 (6.33)	2.21 × 10 ⁻⁴

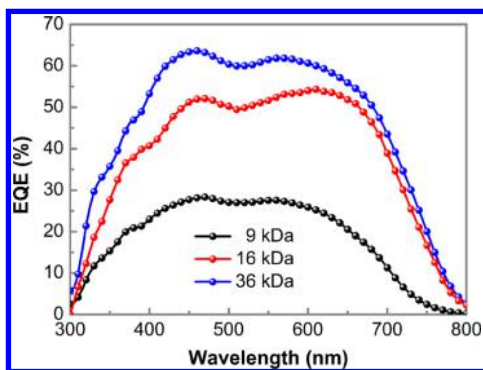


Figure 6. EQE spectra of the solar cells based on different molecular weight PDTs-DTffBT:P₇₁CBM.

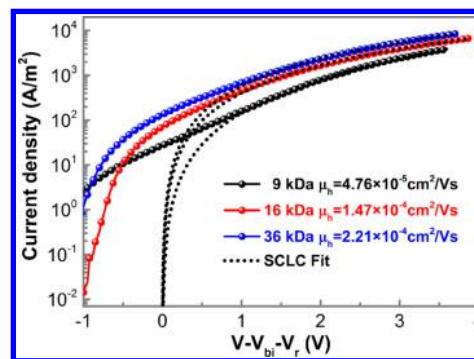


Figure 7. Dark J - V curves of hole-only devices based on PDTs-DTffBT with different molecular weights.

electrodes on each side of the active layer. The current density in the dark (J) was measured by changing the applied voltage V_{appl} from 0 to 5 V. Corresponding J - V curves on a semilogarithmic scale are shown in Figure 7. The hole mobility can be calculated by fitting the resulting curves to the space-charge-limited form, in which the J - V follows the equation of

$$J = \frac{9}{8} \epsilon_0 \epsilon_r \mu_h \frac{V^2}{L^3} \exp\left(0.89\beta \sqrt{\frac{V}{L}}\right)$$

where ϵ_0 is the permittivity of the vacuum, ϵ_r is the relative dielectric constant (typically 3 for conjugated polymers),⁵¹ μ_h is the hole mobility, L is the active layer thickness, and β is the field-dependent factor. V has been corrected by $V = V_{\text{appl}} - V_{\text{bi}} - V_r$, where V_{appl} , V_{bi} , and V_r are the applied bias voltage, built-

in potential, and voltage losses at the electrodes, respectively. The calculated mobility data showed that, when the MW increased from 9 to 16 kDa, the hole mobility increased by a factor of 3. Further increasing MW to 36 kDa, the mobility increased from 1.47×10^{-4} to 2.21×10^{-4} cm² V⁻¹ s⁻¹. These results indicated that the carrier mobility was affected by MW but not linearly dependent. The promoted hole mobility was probably due to the improved π -stacking order and interchain overlap, and the long chains of high MW polymers may also lead to the ordered regions being more electrically connected, facilitating charge transport along the polymer backbone.⁵²⁻⁵⁴ This enhancement was in favor of charge collection and suppressing carrier recombination, accounting for the enlarged J_{SC} and FF of PSCs.

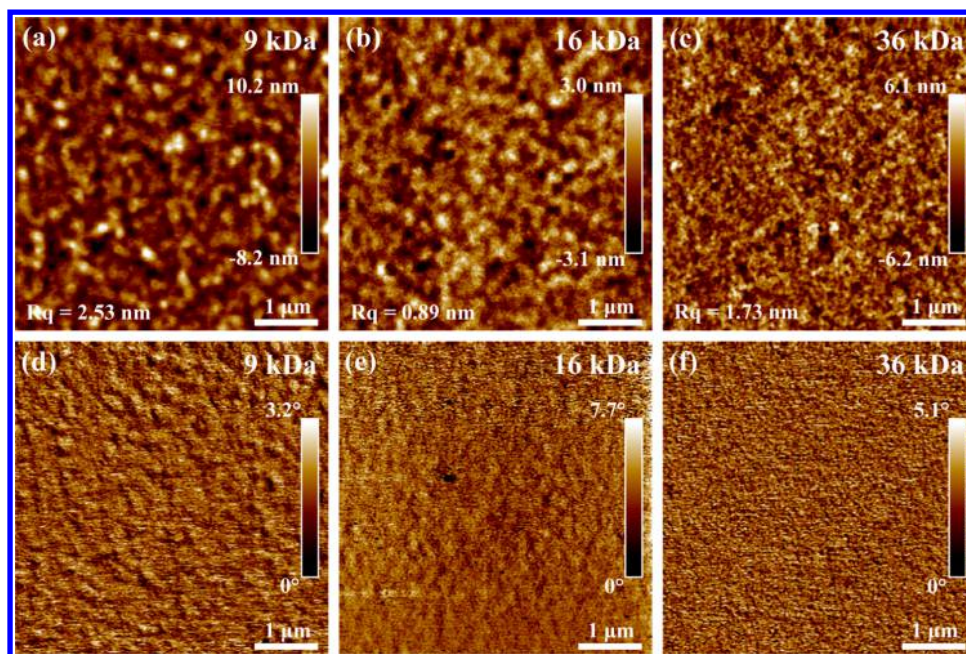


Figure 8. AFM height images (a–c) and phase images (d–f) of the PDTS-DTfBT:PC₇₁BM blend films with a molecular weight of 9 kDa (a, d), 16 kDa (b, e), and 36 kDa (c, f) for PDTS-DTfBT.

3.5. Film Morphology. In addition to the enhanced hole mobility, we demonstrated that the nanoscale morphology evolution as MW increased was also crucial for the photovoltaic properties of devices through an AFM study. Figure 8 shows the AFM height images as well as phase images of PDTS-DTfBT:PC₇₁BM blend films (1:2 weight ratio) with different MW fractions. First, comparing these height images, the mean square surface roughnesses (R_q) of blend films processed by PDTS-DTfBT(9 kDa), PDTS-DTfBT(16 kDa), and PDTS-DTfBT(36 kDa) were 2.53, 0.89, and 1.73 nm, respectively. This suggested that the film surface based on high MW PDTS-DTfBTs (16 and 36 kDa) became much smoother compared with the low MW one, which was favorable for the contact between the active layer and cathode and efficient charge extraction can be expected.^{55,56} Moreover, the phase images in Figure 8 also demonstrate a noticeable difference in the phase separation degree of the three blend films. For the PDTS-DTfBT(9 kDa):PC₇₁BM film, a ridged-like nanoscale morphology can be observed with a relatively big aggregation size of the polymer or fullerene component. This kind of morphology feature was suppressed in the PDTS-DTfBT(16 kDa):PC₇₁BM mixture and finally disappeared when the MW increased to 36 kDa. Apparently, blend film processed by the highest MW PDTS-DTfBT was homogeneous with significantly reduced domain size, implying better miscibility of the polymer and fullerene molecules and larger interfacial area for efficient exciton dissociation.^{56,57} This provided, together with the hole mobility, an explanation for the improved J_{SC} , FF, and photovoltaic performance of the 36 kDa polymer based devices.

4. CONCLUSIONS

In summary, we synthesized low bandgap conjugated polymer PDTS-DTfBTs with three different MWs and investigated the effect of MW on the efficiency of PSCs. The UV–vis absorption spectra and electrochemical cyclic voltammetry measurement showed that the absorption spectra of PDTS-DTfBT were gradually red-shifted and the HOMO energy

level was gradually up-shifted as the MW increased. Furthermore, PDTS-DTfBT with higher MW provided a higher hole mobility and more improved morphology of the PDTS-DTfBT:PC₇₁BM active layer. As a result, the high MW PDTS-DTfBT based PSCs exhibited significantly enhanced J_{SC} and FF; thus, a PCE of 6.40% was achieved. The results highlight the importance of achieving high MW polymers for efficient photovoltaic application.

AUTHOR INFORMATION

Corresponding Authors

*E-mail: sp_wen@jlu.edu.cn. Phone: +86-431-85168242-8221 (S.W.).

*E-mail: rsp1226@gmail.com. Phone: +86-431-85168241-8219 (S.R.).

Notes

The authors declare no competing financial interest.

ACKNOWLEDGMENTS

We would like to acknowledge the financial support from the National Natural Science Foundation of China (Grant Nos. 51303061, 11574110), the Project of Science and Technology Development Plan of Jilin Province (Grant No. 20140204056GX), the Project of Science and Technology Plan of Changchun City (Grant No. 13KG49), and the China Postdoctoral Science Foundation (Grant Nos. 2014T70288, 2013M541299).

REFERENCES

- (1) Yu, G.; Gao, J.; Hummelen, J. C.; Wudl, F.; Heeger, A. J. Polymer Photovoltaic Cells: Enhanced Efficiencies via a Network of Internal Donor-Acceptor Heterojunctions. *Science* **1995**, *270*, 1789–1791.
- (2) Kamat, P. V. Meeting the Clean Energy Demand: Nanostructure Architectures for Solar Energy Conversion. *J. Phys. Chem. C* **2007**, *111*, 2834–2860.
- (3) He, Z. C.; Zhong, C. M.; Su, S. J.; Xu, M.; Wu, H. B.; Cao, Y. Enhanced Power-Conversion Efficiency in Polymer Solar Cells Using an Inverted Device Structure. *Nat. Photonics* **2012**, *6*, 593–597.

- (4) Zhou, Y. H.; Fuentes-Hernandez, C.; Shim, J.; Meyer, J.; Giordano, A. J.; Li, H.; Winget, P.; Papadopoulos, T.; Cheun, H.; Kim, J.; et al. A Universal Method to Produce Low-Work Function Electrodes for Organic Electronics. *Science* **2012**, *336*, 327–332.
- (5) Hwang, I.-W.; Moses, D.; Heeger, A. J. Photoinduced Carrier Generation in P3HT/PCBM Bulk Heterojunction Materials. *J. Phys. Chem. C* **2008**, *112*, 4350–4354.
- (6) Zhou, Y. H.; Fuentes-Hernandez, C.; Shim, J. W.; Khan, T. M.; Kippelen, B. High Performance Polymeric Charge Recombination Layer for Organic Tandem Solar Cells. *Energy Environ. Sci.* **2012**, *5*, 9827–9832.
- (7) Liu, S. J.; Zhang, K.; Lu, J. M.; Zhang, J.; Yip, H.-L.; Huang, F.; Cao, Y. High-Efficiency Polymer Solar Cells via the Incorporation of an Amino-Functionalized Conjugated Metallopolymer as a Cathode Interlayer. *J. Am. Chem. Soc.* **2013**, *135*, 15326–15329.
- (8) You, J. B.; Dou, L. T.; Yoshimura, K.; Kato, T.; Ohya, K.; Moriarty, T.; Emery, K.; Chen, C. C.; Gao, J.; Li, G.; Yang, Y. A Polymer Tandem Solar Cell with 10.6% Power Conversion Efficiency. *Nat. Commun.* **2013**, *4*, 1446.
- (9) Scharber, M. C.; Mühlbacher, D.; Koppe, M.; Denk, P.; Waldau, C.; Heeger, A. J.; Brabec, C. J. Design Rules for Donors in Bulk-Heterojunction Solar Cells—Towards 10% Energy-Conversion Efficiency. *Adv. Mater.* **2006**, *18*, 789–794.
- (10) Li, Y. W.; Xue, L. L.; Li, H.; Li, Z. F.; Xu, B.; Wen, S. P.; Tian, W. J. Energy Level and Molecular Structure Engineering of Conjugated Donor–Acceptor Copolymers for Photovoltaic Applications. *Macromolecules* **2009**, *42*, 4491–4499.
- (11) Wen, S. P.; Dong, Q. F.; Cheng, W. D.; Li, P. F.; Xu, B.; Tian, W. J. A Benzo[1,2-b:4,5-b']dithiophene-Based Copolymer with Deep HOMO Level for Efficient Polymer Solar Cells. *Sol. Energy Mater. Sol. Cells* **2012**, *100*, 239–245.
- (12) Risko, C.; McGehee, M. D.; Brédas, J.-L. A Quantum-chemical Perspective into Low Optical-Gap Polymers for Highly-Efficient Organic Solar Cells. *Chem. Sci.* **2011**, *2*, 1200–1218.
- (13) van Mellekom, H. A. M.; Vekemans, J.; Havinga, E. E.; Meijer, E. W. Developments in the Chemistry and Band Gap Engineering of Donor-Acceptor Substituted Conjugated Polymers. *Mater. Sci. Eng., R* **2001**, *32*, 1–40.
- (14) Zhao, W. C.; Ye, L.; Zhang, S. Q.; Yao, H. F.; Sun, M. L.; Hou, J. H. An Easily Accessible Cathode Buffer Layer for Achieving Multiple High Performance Polymer Photovoltaic Cells. *J. Phys. Chem. C* **2015**, *119*, 27322–27329.
- (15) Wu, J. S.; Cheng, Y. J.; Dubosc, M.; Hsieh, C. H.; Chang, C. Y.; Hsu, C. S. Donor-Acceptor Polymers Based on Multi-fused Heptacyclic Structures: Synthesis, Characterization and Photovoltaic Applications. *Chem. Commun.* **2010**, *46*, 3259–3261.
- (16) Cheng, Y.-J.; Yang, S.-H.; Hsu, C.-S. Synthesis of Conjugated Polymers for Organic Solar Cell Applications. *Chem. Rev.* **2009**, *109*, 5868–5923.
- (17) Wen, S. P.; Pei, J. N.; Zhou, Y. H.; Li, P. F.; Xue, L. L.; Li, Y. W.; Xu, B.; Tian, W. J. Synthesis of 4,7-Diphenyl-2,1,3-Benzothiadiazole-Based Copolymers and Their Photovoltaic Applications. *Macromolecules* **2009**, *42*, 4977–4984.
- (18) Wen, S. P.; Pei, J. N.; Li, P. F.; Zhou, Y. H.; Cheng, W. D.; Dong, Q. F.; Li, Z. F.; Tian, W. J. Synthesis and Photovoltaic Properties of Low-Bandgap 4,7-Dithien-2-yl-2,1,3-Benzothiadiazole-Based Poly(heteroarylenevinylene)s. *J. Polym. Sci., Part A: Polym. Chem.* **2011**, *49*, 2715–2724.
- (19) Wen, S. P.; Cheng, W. D.; Li, P. F.; Yao, S. Y.; Xu, B.; Li, H.; Gao, Y. J.; Wang, Z. L.; Tian, W. J. Synthesis and Photovoltaic Properties of Thieno[3,4-c]pyrrole-4,6-Dione-Based Donor-Acceptor Copolymers. *J. Polym. Sci., Part A: Polym. Chem.* **2012**, *50*, 3758–3766.
- (20) Vohra, V.; Kawashima, K.; Kakara, T.; Koganezawa, T.; Osaka, I.; Takimiya, K.; Murata, H. Efficient Inverted Polymer Solar Cells Employing Favourable Molecular Orientation. *Nat. Photonics* **2015**, *9*, 403.
- (21) Liu, Y. H.; Zhao, J. B.; Li, Z. K.; Mu, C.; Ma, W.; Hu, H. W.; Jiang, K.; Lin, H. R.; Ade, H.; Yan, H. Aggregation and Morphology Control Enables Multiple Cases of High-Efficiency Polymer Solar Cells. *Nat. Commun.* **2014**, *5*, 5293.
- (22) Chen, J. D.; Cui, C. H.; Li, Y. Q.; Zhou, L.; Ou, Q. D.; Li, C.; Li, Y. F.; Tang, J. X. Single-Junction Polymer Solar Cells Exceeding 10% Power Conversion Efficiency. *Adv. Mater.* **2015**, *27*, 1035–1041.
- (23) Nikiforov, M. P.; Lai, B.; Chen, W.; Chen, S.; Schaller, R. D.; Strzalka, J.; Maser, J.; Darling, S. B. Detection and Role of Trace Impurities in High-Performance Organic Solar Cells. *Energy Environ. Sci.* **2013**, *6*, 1513–1520.
- (24) Park, J. K.; Jo, J.; Seo, J. H.; Moon, J. S.; Park, Y. D.; Lee, K.; Heeger, A. J.; Bazan, G. C. End-Capping Effect of a Narrow Bandgap Conjugated Polymer on Bulk Heterojunction Solar Cells. *Adv. Mater.* **2011**, *23*, 2430–2435.
- (25) Katsouras, A.; Gasparini, N.; Koulogiannis, C.; Spanos, M.; Ameri, T.; Brabec, C. J.; Chochos, C. L.; Avgeropoulos, A. Systematic Analysis of Polymer Molecular Weight Influence on the Organic Photovoltaic Performance. *Macromol. Rapid Commun.* **2015**, *36*, 1778–1797.
- (26) Beaupré, S.; Leclerc, M. PCDTBT: en Route for Low Cost Plastic Solar Cells. *J. Mater. Chem. A* **2013**, *1*, 11097–11105.
- (27) Wakim, S.; Beaupré, S.; Blouin, N.; Aich, B.-R.; Rodman, S.; Gaudiana, R.; Tao, Y.; Leclerc, M. Highly Efficient Organic Solar Cells Based on a Poly(2,7-carbazole) Derivative. *J. Mater. Chem.* **2009**, *19*, 5351–5358.
- (28) Intemann, J. J.; Yao, K.; Yip, H.-L.; Xu, Y.-X.; Li, Y.-X.; Liang, P.-W.; Ding, F.-Z.; Li, X. S.; Jen, A. K. Y. Molecular Weight Effect on the Absorption, Charge Carrier Mobility, and Photovoltaic Performance of an Indacenodiselenophene-Based Ladder-Type Polymer. *Chem. Mater.* **2013**, *25*, 3188–3195.
- (29) Tong, M. H.; Cho, S.; Rogers, J. T.; Schmidt, K.; Hsu, B. B. Y.; Moses, D.; Coffin, R. C.; Kramer, E. J.; Bazan, G. C.; Heeger, A. J. Higher Molecular Weight Leads to Improved Photoresponsivity, Charge Transport and Interfacial Ordering in a Narrow Bandgap Semiconducting Polymer. *Adv. Funct. Mater.* **2010**, *20*, 3959–3965.
- (30) Huang, Z. G.; Fregoso, E. C.; Dimitrov, S.; Tuladhar, P. S.; Soon, Y. W.; Bronstein, H.; Meager, I.; Zhang, W. M.; McCulloch, I.; Durrant, J. R. Optimisation of Diketopyrrolopyrrole:Fullerene Solar Cell Performance Through Control of Polymer Molecular Weight and Thermal Annealing. *J. Mater. Chem. A* **2014**, *2*, 19282–19289.
- (31) Kuwabara, J.; Yasuda, T.; Takase, N.; Kanbara, T. Effects of the Terminal Structure, Purity, and Molecular Weight of an Amorphous Conjugated Polymer on Its Photovoltaic Characteristics. *ACS Appl. Mater. Interfaces* **2016**, *8*, 1752–1758.
- (32) Subbiah, J.; Purushothaman, B.; Chen, M.; Qin, T. S.; Gao, M.; Vak, D.; Scholes, F. H.; Chen, X. W.; Watkins, S. E.; Wilson, G. J.; et al. Organic Solar Cells Using a High-Molecular-Weight Benzodithiophene-Benzothiadiazole Copolymer with an Efficiency of 9.4%. *Adv. Mater.* **2015**, *27*, 702–705.
- (33) Liu, C.; Wang, K.; Hu, X. W.; Yang, Y. L.; Hsu, C. H.; Zhang, W.; Xiao, S.; Gong, X.; Cao, Y. Molecular Weight Effect on the Efficiency of Polymer Solar Cells. *ACS Appl. Mater. Interfaces* **2013**, *5*, 12163–12167.
- (34) Vangerven, T.; Verstappen, P.; Drijkoningen, J.; Dierckx, W.; Himmelberger, S.; Salleo, A.; Vanderzande, D.; Maes, W.; Manca, J. V. Molar Mass versus Polymer Solar Cell Performance: Highlighting the Role of Homocouplings. *Chem. Mater.* **2015**, *27*, 3726–3732.
- (35) Schilinsky, P.; Asawapirom, U.; Scherf, U.; Biele, M.; Brabec, C. J. Influence of the Molecular Weight of Poly(3-hexylthiophene) on the Performance of Bulk Heterojunction Solar Cells. *Chem. Mater.* **2005**, *17*, 2175–2180.
- (36) Chu, T.-Y.; Lu, J. P.; Beaupré, S.; Zhang, Y. G.; Pouliot, J.-R.; Zhou, J. Y.; Najari, A.; Leclerc, M.; Tao, Y. Effects of the Molecular Weight and the Side-Chain Length on the Photovoltaic Performance of Dithienosilole/Thienopyrrolodione Copolymers. *Adv. Funct. Mater.* **2012**, *22*, 2345–2351.
- (37) Li, W. T.; Yang, L. Q.; Tumbleston, J. R.; Yan, L.; Ade, H.; You, W. Controlling Molecular Weight of a High Efficiency Donor-Acceptor Conjugated Polymer and Understanding Its Significant Impact on Photovoltaic Properties. *Adv. Mater.* **2014**, *26*, 4456–4462.

- (38) Ma, W.; Yang, G. F.; Jiang, K.; Carpenter, J. H.; Wu, Y.; Meng, X. Y.; McAfee, T.; Zhao, J. B.; Zhu, C. H.; Wang, C.; et al. Influence of Processing Parameters and Molecular Weight on the Morphology and Properties of High-Performance PffBT4T-2OD:PC₇₁BM Organic Solar Cells. *Adv. Energy Mater.* **2015**, *5*, 1501400.
- (39) Kline, R. J.; McGehee, M. D.; Kadnikova, E. N.; Liu, J. S.; Fréchet, J. M. J.; Toney, M. F. Dependence of Regioregular Poly(3-hexylthiophene) Film Morphology and Field-Effect Mobility on Molecular Weight. *Macromolecules* **2005**, *38*, 3312–3319.
- (40) Bartelt, J. A.; Douglas, J. D.; Mateker, W. R.; Labban, A. E.; Tassone, C. J.; Toney, M. F.; Fréchet, J. M. J.; Beaujuge, P. M.; McGehee, M. D. Controlling Solution-Phase Polymer Aggregation with Molecular Weight and Solvent Additives to Optimize Polymer-Fullerene Bulk Heterojunction Solar Cells. *Adv. Energy Mater.* **2014**, *4*, 1301733.
- (41) Wen, S. P.; Wang, C.; Ma, P. F.; Zhao, Y.-X.; Li, C.; Ruan, S. P. Synthesis and Photovoltaic Properties of Dithieno[3,2-b:2',3'-d]silole-Based Conjugated Copolymers. *J. Mater. Chem. A* **2015**, *3*, 13794–13800.
- (42) Wen, S. P.; Wang, C.; Ma, P. F.; Wang, G.; Dong, W.; Gao, Y. J.; Ruan, S. P. Improved Efficiency in Dithieno[3,2-b:2',3'-d]silole-Based Polymer Solar Cells by the Insertion of ZnO Optical Spacer. *J. Phys. Chem. C* **2015**, *119*, 20817–20822.
- (43) Xiao, Z. Y.; Sun, K.; Subbiah, J.; Qin, T. S.; Lu, S. R.; Purushothaman, B.; Jones, D. J.; Holmes, A. B.; Wong, W. W. H. Effect of Molecular Weight on the Properties and Organic Solar Cell Device Performance of a Donor–Acceptor Conjugated Polymer. *Polym. Chem.* **2015**, *6*, 2312–2318.
- (44) Liu, F.; Chen, D.; Wang, C.; Luo, K. Y.; Gu, W. Y.; Briseno, A. L.; Hsu, J. W. P.; Russell, T. P. Molecular Weight Dependence of the Morphology in P3HT:PCBM solar cells. *ACS Appl. Mater. Interfaces* **2014**, *6*, 19876–19887.
- (45) Osaka, I.; Saito, M.; Mori, H.; Koganezawa, T.; Takimiya, K. Drastic Change of Molecular Orientation in a Thiazolothiazole Copolymer by Molecular-Weight Control and Blending with PC₆₁BM Leads to High Efficiencies in Solar Cells. *Adv. Mater.* **2012**, *24*, 425–430.
- (46) Pommerehne, J.; Vestweber, H.; Guss, W.; Mahrt, R. F.; Bässler, H.; Porsch, M.; Daub, J. Efficient Two Layer LEDs on a Polymer Blend Basis. *Adv. Mater.* **1995**, *7*, 551–554.
- (47) Wen, S. P.; Pei, J. N.; Zhou, Y. H.; Xue, L. L.; Xu, B.; Li, Y. W.; Tian, W. J. Synthesis and Photovoltaic Properties of Poly(*p*-phenylenevinylene) Derivatives Containing Oxadiazole. *J. Polym. Sci., Part A: Polym. Chem.* **2009**, *47*, 1003–1012.
- (48) Vandewal, K.; Tvingstedt, K.; Gadisa, A.; Inganäs, O.; Manca, J. V. On the Origin of the Open-Circuit Voltage of Polymer-Fullerene Solar Cells. *Nat. Mater.* **2009**, *8*, 904–909.
- (49) Hou, J. H.; Park, M.-H.; Zhang, S. Q.; Yao, Y.; Chen, L.-M.; Li, J.-H.; Yang, Y. Bandgap and Molecular Energy Level Control of Conjugated Polymer Photovoltaic Materials Based on Benzo[1,2-b:4,5-b']dithiophene. *Macromolecules* **2008**, *41*, 6012–6018.
- (50) Melzer, C.; Koop, E. J.; Mihailetschi, V. D.; Blom, P. W. M. Hole Transport in Poly(phenylene vinylene)/Methanofullerene Bulk-Heterojunction Solar Cells. *Adv. Funct. Mater.* **2004**, *14*, 865–870.
- (51) Campbell, I. H.; Hagler, T. W.; Smith, D. L.; Ferraris, J. P. Direct Measurement of Conjugated Polymer Electronic Excitation Energies Using Metal/Polymer/Metal Structures. *Phys. Rev. Lett.* **1996**, *76*, 1900–1903.
- (52) Himmelberger, S.; Vandewal, K.; Fei, Z. P.; Heeney, M.; Salleo, A. Role of Molecular Weight Distribution on Charge Transport in Semiconducting Polymers. *Macromolecules* **2014**, *47*, 7151–7157.
- (53) Zen, A.; Pflaum, J.; Hirschmann, S.; Zhuang, W.; Jaiser, F.; Asawapirom, U.; Rabe, J. P.; Scherf, U.; Neher, D. Effect of Molecular Weight and Annealing of Poly(3-hexylthiophene)s on the Performance of Organic Field-Effect Transistors. *Adv. Funct. Mater.* **2004**, *14*, 757–764.
- (54) Noriega, R.; Rivnay, J.; Vandewal, K.; Koch, F. P. V.; Stingelin, N.; Smith, P.; Toney, M. F.; Salleo, A. A General Relationship Between Disorder, Aggregation and Charge Transport in Conjugated Polymers. *Nat. Mater.* **2013**, *12*, 1038–1044.
- (55) Ye, L.; Jing, Y.; Guo, X.; Sun, H.; Zhang, S. Q.; Zhang, M. J.; Huo, L. J.; Hou, J. H. Remove the Residual Additives toward Enhanced Efficiency with Higher Reproducibility in Polymer Solar Cells. *J. Phys. Chem. C* **2013**, *117*, 14920–14928.
- (56) Ye, L.; Zhang, S. Q.; Ma, W.; Fan, B. H.; Guo, X.; Huang, Y.; Ade, H.; Hou, J. H. From Binary to Ternary Solvent: Morphology Fine-tuning of D/A Blends in PDPP3T-based Polymer Solar Cells. *Adv. Mater.* **2012**, *24*, 6335–6341.
- (57) Fu, L.; Fu, W. F.; Cheng, P.; Xie, Z. X.; Fan, C. C.; Shi, M. M.; Ling, J.; Hou, J. H.; Zhan, X. W.; Chen, H. Z. A Diketopyrrolopyrrole Molecule End-capped with a Furan-2-carboxylate Moiety: the Planarity of Molecular Geometry and Photovoltaic Properties. *J. Mater. Chem. A* **2014**, *2*, 6589–6597.